

https://doi.org/10.1070/QEL18007

Nonlinear frequency conversion of a Ho:YAG laser beam

K.V. Vorontsov, S.G. Garanin, N.A. Egorov, N.G. Zakharov, R.A. Zorin, V.B. Kolomeets, V.I. Lazarenko, A.S. Nadezhin, G.N. Nomakonov, K.A. Tulyakov, Yu.N. Frolov

Abstract. **We report the results of experiments on frequency conversion of a Ho:YAG laser beam (wavelength $\lambda \sim 2.1$ μm) into the near-, mid-, and far-IR regions, aimed at expanding the spectral composition of compact multispectral sources of coherent radiation. The experimentally found laser conversion efficiency into the second harmonic reaches 32% and 54% in the cw and repetitively pulsed regimes, respectively. The parametric conversion efficiency into the mid-IR range (λ = 3.5–5.0 μm) reaches 55%, while for the far-IR range (λ = 8–8.2 μm) it turns out to be 10.5%.**

Keywords: *Ho:YAG laser, nonlinear conversion, second-harmonic generator, optical parametric oscillator.*

1. Introduction

To solve a number of applied problems, e.g., remote sensing of atmosphere, one needs compact multispectral sources of near-, mid-, and far-IR coherent radiation. The operation of these devices is based on efficient nonlinear conversion of radiation of a well-developed laser source into the desired wavelength range. For example, holmium laser radiation with a wavelength $\lambda \sim 2.1$ μm can be converted both into the wavelength range near 1 μm and lower (by generating the second and subsequent harmonics) and into the spectral range of 3–12 μm due to the parametric radiation conversion. This approach makes it possible to simplify significantly the design of a unified multispectral laser system by excluding individual emitters from its composition.

Based on the results of the studies published in the period from 2010 to 2021, one can conclude the following: currently, the most attractive approach to the design of compact sources with nonlinear conversion of 2-μm radiation implies pumping of a repetitively pulsed Ho:YAG laser by cw radiation of solid-state or fibre thulium lasers with subsequent nonlinear frequency conversion using an optical parametric oscillator (OPO) based on a nonlinear $ZnGeP_2$ crystal or a harmonic generator based on a periodically poled $LiNbO_3$ (PPLN) crystal. This scheme has advantages over similar designs in the efficiency, output power, and technological sophistication of the components in use. Its main advantage is the high conversion efficiency of consumed electrical energy into the radiation energy, simple design, and possibility of generating beams of high optical quality. Of extreme importance are the factors of power consumption and the weight and size characteristics, because these parameters are crucial for mobile applications, for example, in ecological monitoring systems.

In particular, the efficiency of converting radiation of fibre or solid-state Tm:YLF lasers into Ho:YAG laser radiation reaches 55%–70% [1, 2]. The conversion efficiency of repetitively pulsed holmium laser radiation into the second harmonic exceeds 50% [3]. The conversion efficiency of 2-μm radiation into the wavelength range of 3.5–5 μm in parametric oscillators and amplifiers is 50%–60% [4, 5]. OPOs are also widely used in design of far-IR sources. A possibility of converting 2-μm Ho:YAG laser radiation with a pulse repetition rate of 20 kHz into the far-IR (8–10 μm) region in an OPO based on nonlinear $ZnGeP_2$ crystal was shown in [6]. The maximum output power at a wavelength of ~8 μm was obtained with a conversion efficiency of 10.7% and quantum efficiency of 41%. The possibility of achieving a high output power in a $ZnGeP_2$-based OPO in the wavelength range of 9.6–10.6 μm by increasing the 2-μm pump power was shown in [7]. However, the parametric generation threshold increased significantly in this case, and the maximum conversion efficiency of pump radiation into the long-wavelength region with λ = 9.8 μm was as low as ~3.9%.

The first experiments on nonlinear radiation conversion in GaSe and $ZnGeP_2$ crystals were performed at the Institute for Laser Physics Research "RFNC–VNIIEF" in cooperation with colleagues from the Institute for Monitoring Climatic and Ecological Systems of the Russian Academy of Sciences, as early as at the beginning of the 1990s [8]. In 2005, as a result of the joint research with the Institute of Applied Physics of the Russian Academy of Sciences (Nizhny Novgorod), parametric generation was implemented in a $ZnGeP_2$ crystal pumped by 2-μm radiation [9]. Further efforts were aimed at developing nonlinear converters as components of mobile laser sources for solving specific applied problems. The main purpose of our study was to obtain nonlinear conversion efficiency in devices not inferior to that of the laboratory samples described in the aforementioned papers.

K.V. Vorontsov, S.G. Garanin, N.A. Egorov, V.B. Kolomeets, A.S. Nadezhin, G.N. Nomakonov, Yu.N. Frolov Russian Federal Nuclear Centre – All-Russian Research Institute of Experimental Physics (RFNC–VNIIEF), prosp. Mira 37, 607188 Sarov, Nizhny Novgorod region, Russia;
N.G. Zakharov, R.A. Zorin, V.I. Lazarenko Russian Federal Nuclear Centre – All-Russian Research Institute of Experimental Physics (RFNC–VNIIEF), prosp. Mira 37, 607188 Sarov, Nizhny Novgorod region, Russia; Lobachevsky State University of Nizhny Novgorod, prosp. Gagarina 23, 603950 Nizhny Novgorod, Russia;
e-mail: dikaion@yandex.ru;
K.A. Tulyakov Russian Federal Nuclear Centre – All-Russian Research Institute of Experimental Physics (RFNC–VNIIEF), prosp. Mira 37, 607188 Sarov, Nizhny Novgorod region, Russia; Lomonosov Moscow State University, Leninskie Gory 1, 119991 Moscow, Russia

Received 15 December 2021
Kvantovaya Elektronika **52** (3) 262–268 (2022)
Translated by Yu.P. Sin'kov

2. SHG experiments

2.1. Radiation source

In all the SHG and OPO experiments described below the pump source for nonlinear radiation converters was a Ho:YAG laser, generating radiation with a wavelength of 2.091 μm ($\Delta\lambda \sim 0.5$ nm) on the fundamental mode of stable resonator (beam quality factor $M^2 \sim 1.1$), formed by plane and spherical mirrors. The spectral distribution of Ho:YAG laser intensity is presented in Fig. 1.

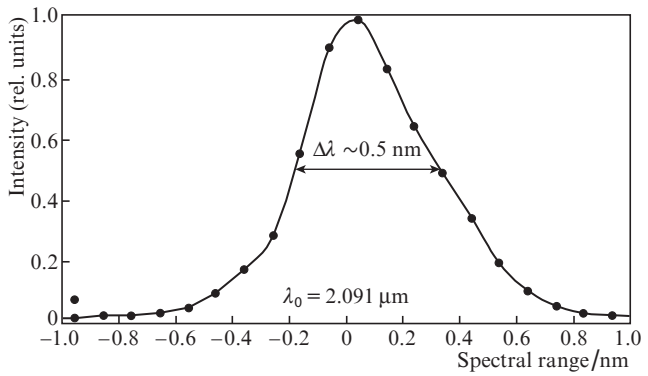

Figure 1. Spectral distribution of Ho:YAG laser radiation intensity.

Q-switching of the resonator using an acousto-optic modulator located in it made it possible to generate repetitively pulsed radiation with a variable pulse repetition rate. The FWHM of generated pulses depended almost linearly on their repetition rate. A dependence of the Ho:YAG-laser pulse duration on the pulse repetition rate is shown in Fig. 2.

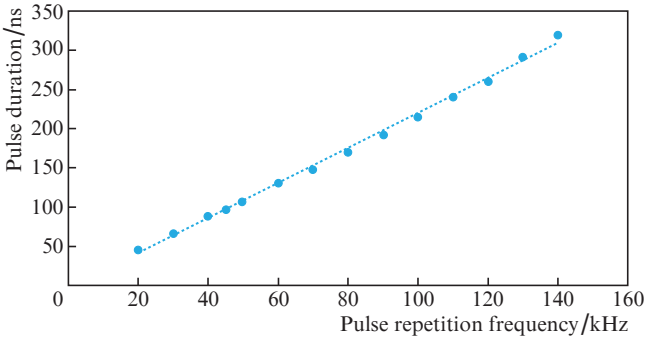

Figure 2. (Colour online) Dependence of the Ho:YAG-laser pulse duration on the pulse repetition rate.

2.2. Second-harmonic generation

Experiments on second-harmonic generation in a Ho:YAG laser were performed in both cw and repetitively pulsed regimes. In both cases a PPLN crystal with a length of 40 mm and polarisation period $\Lambda = 31.6$ μm served as a nonlinear element. The phase matching tuning was performed by changing the crystal temperature. The maximum value of second-harmonic conversion efficiency was obtained at a crystal temperature of ~93 °C.

In the cw SHG experiments the holmium laser beam was focused into the nonlinear crystal centre. The radiation intensity in the beam waist, $I_{cw} = P_m/S_{eff}$, was varied by increasing the average power P_m of the Ho:YAG laser (S_{eff} is the waist area). The experimental dependence of second-harmonic conversion efficiency on the intensity of the cw Ho:YAG laser beam in the waist is shown in Fig. 3.

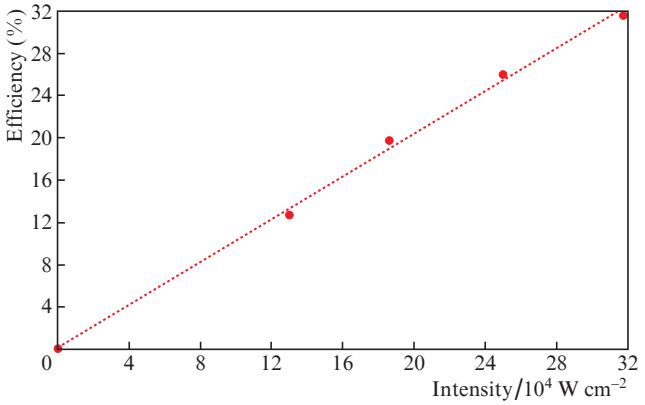

Figure 3. (Colour online) Experimental dependence of the conversion efficiency of cw Ho:YAG laser radiation into the second harmonic on the laser radiation intensity in the beam waist.

It can be seen that the conversion efficiency is ~10%/(10^5 W cm^{-2}); the dependence remains linear in the experimentally available range of variation in radiation intensity. Figure 4 shows calculated and experimental dependences of the relative conversion efficiency on the crystal temperature at a maximum pump power. The calculation model used by us, described as the "split-step method" in [10], implied alternating calculation of the nonlinear interaction and diffraction of the pump and second harmonic beams in the crystal for each longitudinal pump mode. As can be seen in Fig. 4, the FWHM value for the peak of the temperature dependence of conversion efficiency is ~4.5 °C.

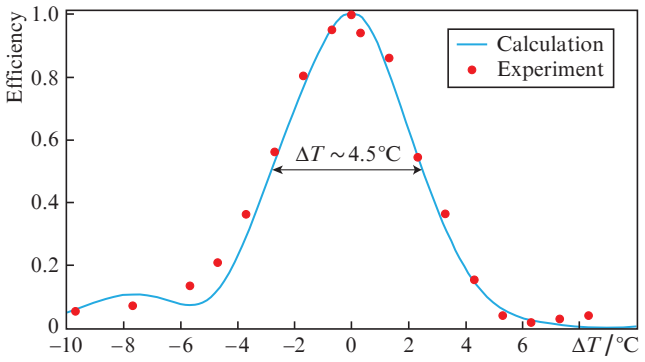

Figure 4. (Colour online) Calculated and experimental dependences of relative conversion efficiency of cw Ho:YAG laser radiation into the second harmonic on the variation in crystal temperature.

In the experiments on pulsed SHG, the repetitively pulsed beam of a holmium laser was also focused into the centre of nonlinear crystal. The pump intensity in the waist, $I_{imp} = E_{imp}/(t_{imp}S_{eff})$, was varied by changing the pulse repetition

rate. The pulse energy E_{imp} decreased inversely proportionally to rate, because the pulse duration t_{imp} depended linearly on the pulse repetition rate (see Fig. 2). The average pump power did not change in the experiment. The experimental dependence of second-harmonic conversion efficiency on the intensity of repetitively pulsed Ho:YAG laser beam in the waist is shown in Fig. 5; this dependence demonstrates that

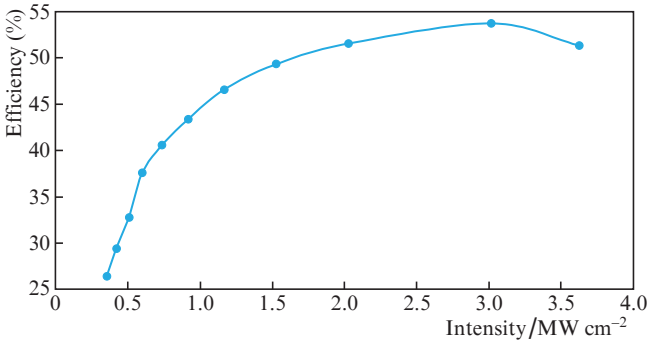

Figure 5. (Colour online) Experimental dependence of the second-harmonic conversion efficiency on the intensity of repetitively pulsed Ho:YAG laser radiation in the beam waist.

the maximum conversion efficiency reaches ~54% at a power density of ~3 MW cm^{-2}. The dependence saturates at this value and then falls off. Figure 6 shows the calculated and experimental dependences of relative conversion efficiency on variation in the crystal temperature at the maximum pump power available in the experiment. It can be seen that the FWHM of the temperature dependence peak is ~4.1°C.

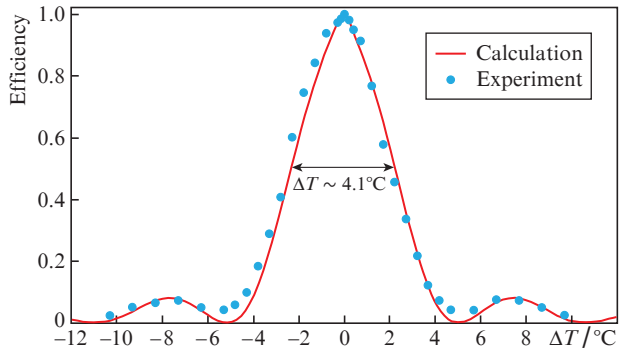

Figure 6. (Colour online) Calculated and experimental dependences of relative conversion efficiency of repetitively pulsed Ho:YAG laser radiation on variation in crystal temperature.

3. Parametric generation of light

The experiments on nonlinear conversion of pump radiation into the long-wavelength spectral region were performed using an OPO based on a nonlinear $ZnGeP_2$ crystal (ZGP) placed in a compact three-mirror ring cavity, whose optical scheme is presented in Fig. 7. Pumping was carried out by a repetitively pulsed Ho:YAG laser with a pulse repetition rate of 20 kHz. The conversion efficiency was optimised by matching the optical lengths of OPO and three-mirror ring cavity,

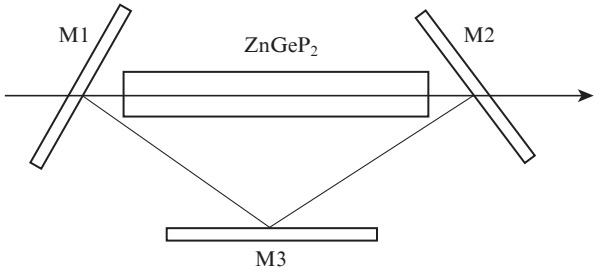

Figure 7. Optical scheme of the OPO ring cavity: (M1) input mirror; (M2) output mirror; (M3) totally reflecting mirror.

which made it possible to reduce significantly the lasing threshold due to the suppression of fluctuations of interacting-wave phase relations [11]. The optimisation procedure will be considered in detail below when describing the experiments on nonlinear conversion of a Ho:YAG laser beam into the mid-IR region.

3.1. OPO calculation model

The OPO calculation model was elaborated in order to estimate the decrease in the parametric generation threshold from the point of view of expediency of applying the method of matching optical cavity lengths in a specific product, as well as determining the necessary accuracy of adjusting the position of optical elements to set initial data for designing optomechanical units entering the cavity composition.

Since the range of problems solved using this model is rather limited, the following simplifications were made: spatial effects were disregarded (i.e., the interacting components of electric field were considered in the plane-wave approximation), and it was assumed that the interacting components propagate with the same speed in a nonlinear crystal and bypass the OPO cavity for the same time. Proceeding from the above assumptions, we took as a basis the simplest mathematical model of an OPO [12], which describes the interaction of three electric field components: amplitudes of the pump field (E_0) and the short-wavelength (E_1) and long-wavelength (E_2) generation components. The interacting field wavelengths (in vacuum) are related by the energy conservation law:

$$1/\lambda_0 = 1/\lambda_1 + 1/\lambda_2. \quad (1)$$

The wave propagation in a nonlinear crystal is described by the equations

$$\partial E_0/\partial z = \mathrm{i}\eta_0 E_1 E_2 \exp(-\mathrm{i}\Delta k z), \quad (2)$$

$$\partial E_1/\partial z = \mathrm{i}\eta_1 E_0 E_2^* \exp(\mathrm{i}\Delta k z), \quad (3)$$

$$\partial E_2/\partial z = \mathrm{i}\eta_2 E_0 E_1^* \exp(\mathrm{i}\Delta k z), \quad (4)$$

where $\eta_{0,1,2} = 2\pi k_{0,1,2} d_{\mathrm{eff}}/n_{0,1,2}^2$; $k_{0,1,2} = 2\pi n_{0,1,2}/\lambda_{0,1,2}$; $\Delta k = k_0 - k_1 - k_2$; $n_{0,1,2}$ is the refractive index for the three field components; d_{eff} is the effective nonlinearity of interaction; and z is the distance from the crystal input face.

The time dependence of the pump field amplitude on the crystal input face is determined by the pulse shape and average pump energy density. The amplitudes of generation fields at the crystal input are the sums of pseudorandom noise component and the amplitudes of components transmitted through the crystal with allowance for the cavity round-trip time, loss on optical elements, and accumulated phase difference.

In the case of monochromatic pumping the inclusion of N pairs of generation components, satisfying expression (1), into the model expands the system of equations (2)–(4) to $2N + 1$ equations:

$$\partial E_0/\partial z = \mathrm{i}\eta_0 \sum_n E_{1n}E_{2n}\exp(-\mathrm{i}\Delta k_n z), \quad (5)$$

$$\partial E_{1n}/\partial z = \mathrm{i}\eta_{1n}E_0E_{2n}^*\exp(\mathrm{i}\Delta k_n z), \quad (6)$$

$$\partial E_{2n}/\partial z = \mathrm{i}\eta_{2n}E_0E_{1n}^*\exp(\mathrm{i}\Delta k_n z), \quad (7)$$

where n is the number of the pair of interacting generation components.

The consideration of pump radiation in the form of M longitudinal modes as discrete (quantum) components makes it necessary to solve $N + MN + M$ equations as a minimum, because each pump mode with a wavelength λ_{0m} calls for its own set of generation modes satisfying expression (1). However, since several hundreds of longitudinal pump modes were taken into account in our calculations, we rejected discrete pump modes in favour of simplification, which assumes exclusively classical representation of the pump field. And, since the spectral width (less than 1 nm) of the pump radiation used in our experiments is much smaller than the parametric generation spectral width (several hundreds of nanometres), one can consider the wavelengths of different pump modes to be approximately equal to λ_0 and restricted to one set of generation modes.

Let the pump radiation consist of M modes, whose electric field depends on time t as

$$A_m\exp\{\mathrm{i}2\pi[c/(\lambda_0 \pm \Delta\nu m)]t + \mathrm{i}\varphi_m\}, \quad (8)$$

where m is an integer, A_m is a coefficient taking into account the distribution of pump energy between modes, c is the speed of light, $\Delta\nu$ is the spectral range between pump laser cavity modes, and φ_m is the phase. Let us rewrite expression (8) in the form

$$A_m\exp\{\mathrm{i}2\pi c/[\lambda_0 + \mathrm{i}(\varphi_m \pm 2\pi\Delta\nu mt)]\}, \quad (9)$$

In other words, we consider the pump radiation as a set of fields with a wavelength λ_0, whose phase periodically changes with time. Then the expression for the pump field amplitude can be written as

$$E_0 = \sum_m A_m\exp[\mathrm{i}(\varphi_m \pm 2\pi\Delta\nu mt)]. \quad (10)$$

The coefficients A_m are determined from the experimental pump spectrum. The pump mode phases φ_m are set randomly before calculating the transmission of each pump pulse through the OPO. The simulation results are obtained by averaging the calculation data for no less than 100 pulses.

The number N of generation component pairs is determined by the expected generation spectral width and the spectral range between OPO cavity modes. It is assumed for simplicity that the wavelengths of short-wavelength components coincide with those of OPO cavity modes. The wavelengths of long-wavelength components are calculated using expression (1).

3.2. Parametric generation of radiation in the range of 3.5–5 μm

Experiments were performed on a $ZnGeP_2$ crystal having a size of $6 \times 6 \times 20$ mm and an optical axis making an angle $\theta = 54.5°$ with the pump beam direction (eeo synchronism). Input cavity mirror M1 (Fig. 7) had a high transmittance for pump radiation with $\lambda = 2.1$ μm and a high reflectance in the range of generation with $\lambda = 3.5 - 5.0$ μm. Output mirror M2 had a high transmittance for the pump radiation and a reflectance of ~ 50% at the generation wavelength. Mirror M3 had a high reflectance in the generation range. The cavity physical length was ~70 mm.

Figure 8 shows the calculated and experimental dependences of relative parametric generation threshold on the increment in the physical length of pump laser cavity. Both the calculation and experiment demonstrate a significant (by a factor of about 1.5) decrease in the parametric generation threshold at exact matching of cavity lengths for the pump laser and OPO (at $\Delta L = 0$). The experimental peak half-width was ΔL ~1.3 mm, whereas the calculation showed a smaller ΔL value (~0.8 mm). The peak half-width is equal to the increment (change from zero to both sides) of the physical cavity length.

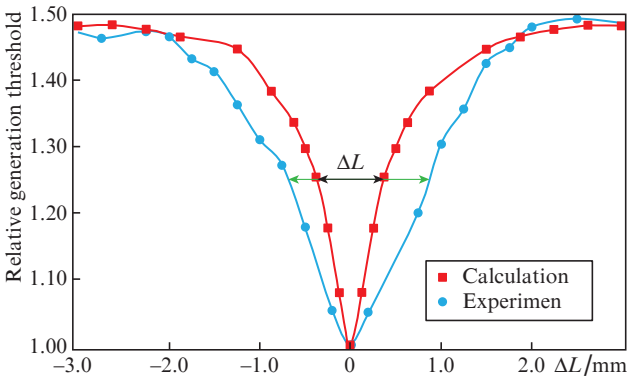

Figure 8. (Colour online) Calculated and experimental dependences of relative parametric generation threshold on the increment in the physical length of pump laser cavity.

Figure 9 shows the calculated and experimental spectra of short- and long-wavelength parametric generation components at $\Delta L = 0$ (cavity length matching regime); the same spectra at $\Delta L = -2$ mm (in the absence of matching) are presented in Fig. 10. One can see that, at $\Delta L = 0$, the spectra exhibit a pronounced periodic structure (a set of clusters), which indicates suppression of phase-relation fluctuations when matching the round-trip times of the pump laser and OPO cavities and is accompanied by a significant decrease in

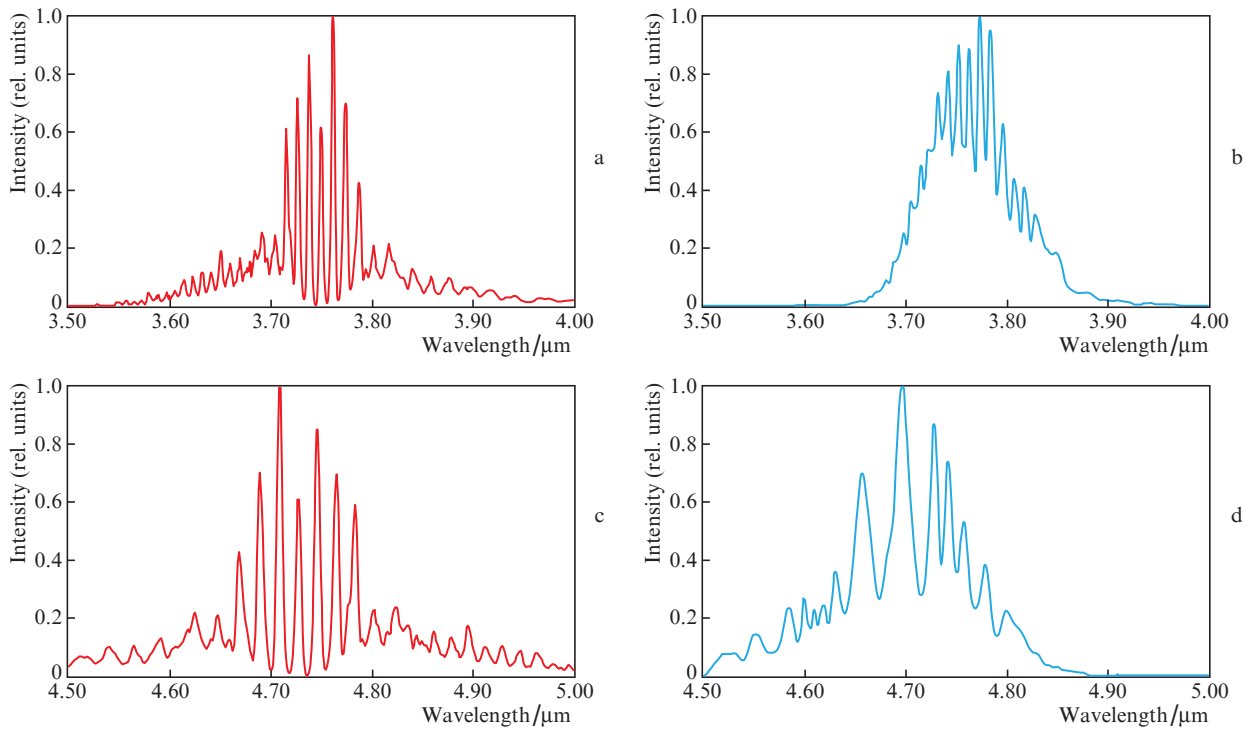

Figure 9. (Colour online) (a, c) Calculated and (b, d) experimental spectra of (a, b) short-wavelength and (c, d) long-wavelength components of parametric generation in the regime of matched pump laser and OPO cavity lengths ($\Delta L = 0$).

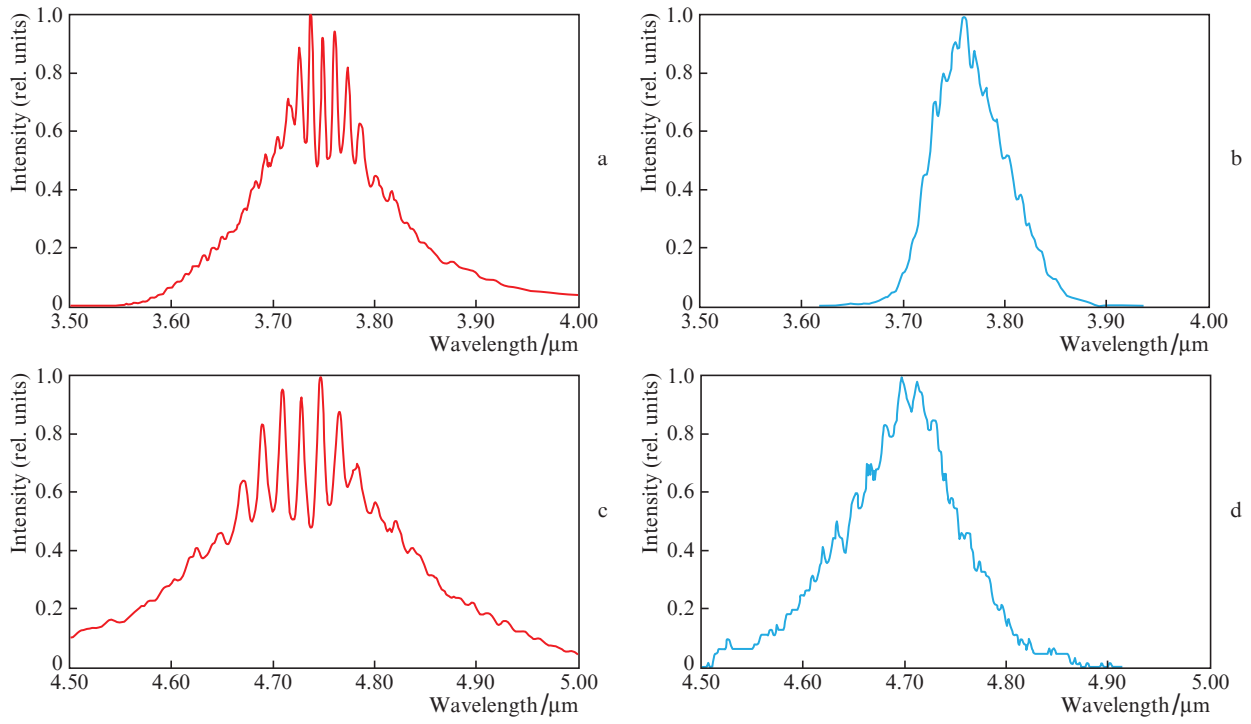

Figure 10. (Colour online) (a, c) Calculated and (b, d) experimental spectra of (a, b) short-wavelength and (c, d) long-wavelength components of parametric generation in the absence of matching of pump laser and OPO cavity lengths (the increment in the pump laser cavity length is $\Delta L = -2$ mm).

the parametric generation threshold. At the same time, in the absence of matching (at $\Delta L = -2$ mm), one can observe a diffusion of the periodic structure of parametric-generation spectral clusters.

An analysis of the presented figures shows that the calculation results are on the whole consistent with the experimental data, and the model makes it possible to estimate the level of reducing the generation threshold and determine the accu-

racy with which the optical elements must be arranged when matching the optical lengths of pump laser and OPO cavities. However, there are also some discrepancies. First, the peak widths in the experimental dependences (either cluster structures or measured values of generation threshold) are larger than the calculated estimates by a factor of about 1.5. Second, in the mismatched regime ($\Delta L \neq 0$), the experimental spectrum of parametric generation is somewhat narrower than the calculated one.

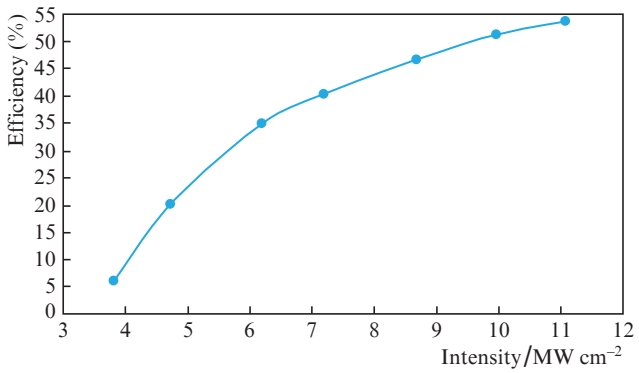

Figure 11. (Colour online) Dependence of the conversion efficiency of repetitively pulsed Ho:YAG laser radiation into the mid-IR range on the pump radiation intensity in the beam waist.

The broadening of the experimental peaks in comparison with the calculated one can be explained by the numerous simplifications accepted in the model to describe the nonlinear interaction. The narrower parametric generation spectrum (in comparison with the calculated one) in the mismatched regime is explained, in our opinion, by the intracavity losses, which are disregarded in the calculation model. In the matched regime, no generation was observed in the spectral range of 4.8–5.0 μm in both the calculated and experimental spectra. In the mismatched regime, absorption of atmospheric gases in the aforementioned spectral region impedes the development of both the idler wave and the corresponding signal wave in the range of 3.6–3.7 μm, due to which a discrepancy between the calculated and experimental data arises.

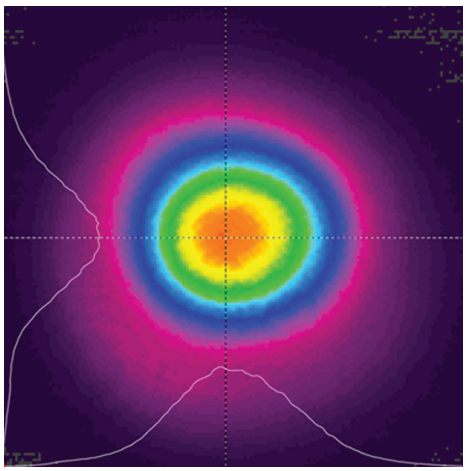

Figure 12. (Colour online) Parametric generation in the far-field zone.

Figure 11 shows a dependence of the efficiency of converting the repetitively pulsed Ho:YAG laser radiation into the mid-IR range on the radiation intensity in the pump beam waist. An image of the far-field zone of parametric generation is presented in Fig. 12.

3.3. Parametric generation in the vicinity of 8 μm

Experiments were performed on a $ZnGeP_2$ crystal having a size of 6 × 6 × 12 mm and optical axis oriented at an angle $\theta = 51.5°$ (eeo-synchronism).

Input cavity mirror M1 (see Fig. 7) had a high transmittance for the pump radiation at $\lambda = 2.1$ μm and a high reflectance in the short-wavelength range of OPO radiation at $\lambda = 2.7–2.9$ μm. Output mirror M2 had a high transmittance for the pump radiation and long-wavelength component, $\lambda = 7.5–8.5$ μm, and its reflectance for the short-wavelength component was ~95%. Mirror M3 had a high reflectance in the short-wavelength generation range. The cavity physical length was ~50 mm.

The radiation divergence measured at the output of telescope with a sixfold magnification turned out to be $\sim 2.5 \times 10^{-3}$ rad. Figure 13 shows the dependence of the conversion efficiency of repetitively pulsed Ho:YAG laser radiation into the far-IR range on the radiation intensity in the pump beam waist.

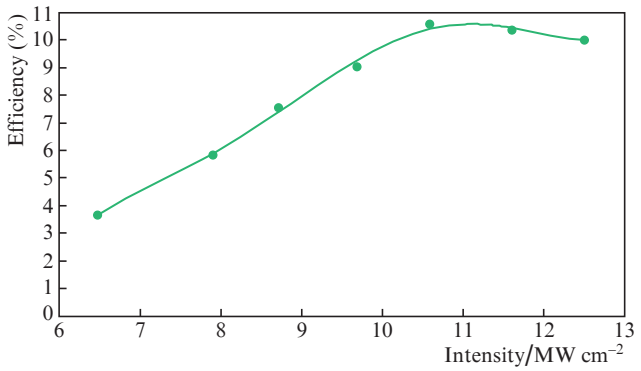

Figure 13. (Colour online) Dependence of the conversion efficiency of repetitively pulsed Ho:YAG laser radiation into the far-IR range on the pump radiation intensity in the beam waist.

Figure 14 presents oscillograms of pump laser and OPO pulses for the idler wave at $\lambda \sim 8.1$ μm. The pulse durations at an intensity level of 0.5 (0.1) were 37 (81) ns for the pump radiation and 33 (56) ns for the OPO idler wave. As can be seen in the figure, the OPO pulse leading edge is much steeper than that of the pump pulse.

The spectral distribution of OPO intensity was recorded by a monochromator with a resolution $\Delta\lambda \approx 2$ nm. Figure 15 shows the idler wave spectra in the vicinity of 8 μm at different crystal temperatures, which demonstrate a blue shift of spectral maximum from ~ 8150 to 7990 nm with an increase in temperature from 10 to 40°C, which corresponds to the coefficient $\Delta\lambda/\Delta T \approx 5.3$ nm deg^{-1}. The signal wave radiation is red-shifted in this case.

The spectral widths of the intensity distribution at a level of 0.5 (0.1) of the maximum $\Delta\lambda_{0.5}$ ($\Delta\lambda_{0.1}$) were 160 (310), 140

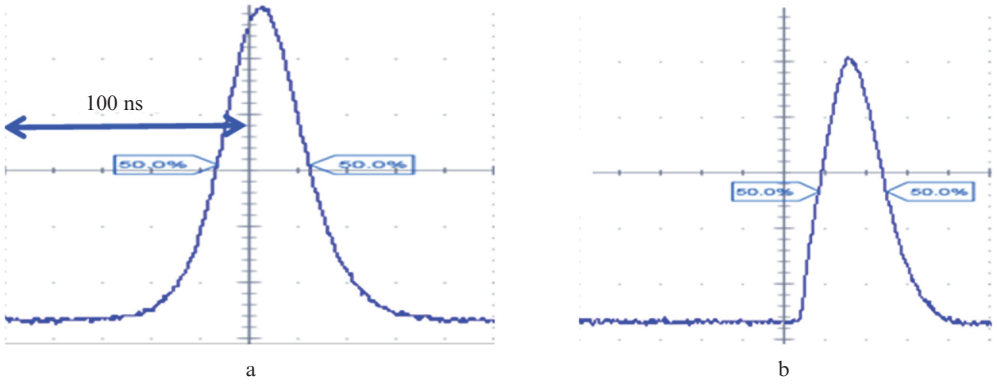

Figure 14. (Colour online) Oscillograms of pulses of (a) pump laser radiation at λ ~2 μm and (b) an OPO idler wave at λ ~8.1 μm.

(270), and 125 (255) nm at temperatures of 10, 20, and 40 °C, respectively. Thus, the width of the spectral distribution at the base level is almost two times larger than the half-width. Note that, along with the idler wave radiation, a weak residual pump radiation at λ ~2.1 μm and signal wave radiation at λ ~2.83 μm with a half-width $\Delta\lambda_{0.5}$ ~55 nm were registered at the OPO output.

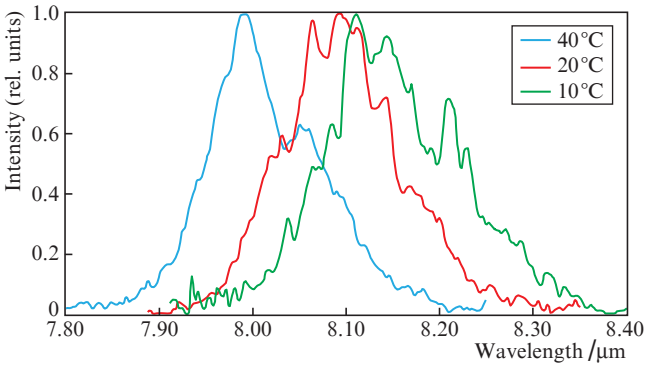

Figure 15. (Colour online) Idler wave spectra at crystal temperatures of 10, 20, and 40 °C.

4. Conclusions

When studying the nonlinear converters of Ho:YAG laser radiation, we developed technical solutions that made it possible to master the production of compact multispectral sources of coherent radiation in the near-, mid-, and far-IR regions, which became a basis for further numerous multipurpose developments; some technical solutions are protected by patents [13, 14]. The efficiency of the developed converters is not inferior to that of laboratory samples [3–7]. The experimentally obtained conversion efficiency of Ho:YAG laser radiation into the second harmonic achieved 32% and 54% in the cw and repetitively pulsed regimes, respectively. The parametric conversion efficiency into the mid-IR (3.5–5 μm) and far-IR (8–8.2 μm) regions achieved 55% and 10.5%, respectively.

Acknowledgements. This work was supported by the national project 'Science and Universities' (No. FSWR-2021–012) due to the federal budget subsidy to support the state task for research.

References

1. Zakharov N.G., Antipov O.L., Sharkov V.V., Savikin A.P. *Quantum Electron.*, **40** (2), 98 (2010) [*Kvantovaya Elektron.*, **40** (2), 98 (2010)].
2. Gaoyou Liu, Shuyi Mi, Ke Yang, Disheng Wei, Junhui Li, Baoquan Yao, Chao Yang, Tongyu Dai, Xiaoming Duan, Lixin Tian, Youlun Ju. *Opt. Lett.*, **46** (1), 82 (2021).
3. Bethel M., Dergachev A., Petrov D., in *Lasers Congress 2016 (ASSL, LSC, LAC), OSA Techn. Digest* (online) (Optica Publishing Group, 2016) paper JTu2A.19.
4. Chuan-Peng Qian, Bao-Quan Yao, Ben-Rui Zhao, Gao-You Liu, Xiao-Ming Duan, Tong-Yu Dai, You-Lun Ju, Yue-Zhu Wang. *Opt. Lett.*, **44** (3), 715 (2019).
5. Lippert Espen, Fonnum Helge, Haakestad Magnus W. *Proc. SPIE*, **9251**, 92510D (2014).
6. Lippert E., Rustad G., Arisholm G., Stenersen K. *Opt Express*, **16** (18), 13884 (2008).
7. Gao-You Liu, Yi Chen, Bao-Quan Yao, Rui-xue Wang, Ke Yang, Chao Yang, Shu-yi Mi, Tong-Yu Dai, Xiao-Ming Duan. *Opt. Lett.*, **45** (8), 2347 (2020).
8. Andreev Yu.M., Velikanov S.D., Elutin A.S., Zapol'skii A.F., Frolov Yu.N, et al. *Quantum Electron.*, **19** (11), 1035 (1992) [*Kvantovaya Elektron.*, **19** (11), 1010 (1992)].
9. Antipov O.L., Eremeykin O.N., Frolov Yu.N., Freidman G.I., Garanin S.G., Il'kaev R.I., Konyushkov F.P., Lasarenko V.I., Mischenko G.M., Savikin A.P., Sergeev A.M., Velikanov S.D., Volkov R.Yu., in *Proc of Int. Symposium "Topical Problems of Nonlinear Wave Physics"* (NWP-2005) (2005) pp 9, 10.
10. Arisholm G. *J. Opt. Soc. Am. B*, **14** (10), 2543 (1997).
11. Arisholm G. et al. *Opt. Lett.*, **25** (22), 1654 (2000).
12. Tang C.L., Cheng L.K. *Laser Sci. Technol. – An Internat. Handbook* (Hardwood Academic Publisher, 1995).
13. Frolov Yu.N., Glukhodedov V.D., Galashin Yu.A., Sin'kov S.D. RU Patent No. 2688860 (priority date 24 May, 2018).
14. Zakharov N.G., Vorontsov K.V., Frolov Yu.N., Lazarenko V.I., Nadezhin A.S., Mukhin A.V., Glukhodedov V.D. RU Patent No. 2704568 (priority date 18 July, 2019).